An Uncertainty Estimation Exercise for Two-dimensional Steady incompressible flow

Yohei Sato* and Takanori Hino*

*National Maritime Research Institute, Center for CFD Research,
6-38-1,Shinkawa, Mitaka, Tokyo, 181-0004, JAPAN
E-mail: satoyoh@nmri.go.jp, hino@nmri.go.jp

I. INTRODUCTION

The necessity of the numerical uncertainty estimation of Computational Fluid Dynamics (CFD) solutions has been increasing in recent years in order to evaluate the accuracy of CFD analyses which are used in practical designs of a ship hull or other engineering devices. In generally, results of CFD largely depend on quality and size of a grid, therefore the convergence behavior with qualified grids should be studied.

This paper reports the numerical uncertainty estimation for the two-dimensional, steady, incompressible, turbulent flows over a hill and a backward facing step (ERCOFTAC Database, Case-18 and 30). The flow fields are analyzed with the Navier-Stokes solver SURF, which is being developed at National Maritime Research Institute. The uncertainty estimation procedure which is proposed by Eca and Hoekstra [1],[2] is used for the uncertainty analysis. This estimation procedure is based on the concept of Grid Convergence Index proposed by Roache[3].

The paper is organized as follows. Following the description of the numerical method in Part II, Part III describes the boundary conditions. In Part IV, the uncertainty estimation procedure is outlined. In Part V, the results of uncertainty analysis are described, and these results are discussed in Part VI. The final part, Part VII, is the conclusions.

II. NUMERICAL METHOD

In this section, we briefly summarize a numerical method used. A finite-volume method with an unstructured grid for three-dimensional Navier-Stokes equations, SURF[4], is employed.

The governing equations are three-dimensional incompressible Navier-Stokes equations.

Spatial discretization is based on a finite-volume method. A solution domain is divided into cells. A cell shape is polyhedron: tetrahedron, hexahedron, prism or pyramid. The cell-centered layout is adopted, in which the flow variables (p,u,v,w) are defined at a center of each cell. The control volume for each cell is a cell itself.

The artificial compressibility approach proposed by Chorin [5] is employed in the present scheme to couple the velocity and pressure fields. Usually, in this approach the term $\frac{1}{\beta}\frac{\partial p}{\partial t}$ is added to the continuity equation, where β is a parameter of artificial compressibility.

The equations to be solved have the form as follows:

$$\frac{\partial V_i q_i}{\partial t} + \sum_{faces}\left(E - E^v\right) = 0 \qquad (1)$$

where

$$q_i = \frac{\int_{Vi} q^n dV}{Vi},$$

$$E = \tilde{e}S_x + \tilde{f}S_y + \tilde{g}S_z,\ E^v = e^v S_x + f^v S_y + g^v S_z,$$

$$q = \begin{bmatrix} p \\ u_1 \\ u_2 \\ u_3 \end{bmatrix}, \tilde{e} = \begin{bmatrix} \beta u \\ u_1u_1 + p \\ u_2u_1 \\ u_3u_1 \end{bmatrix}, \tilde{f} = \begin{bmatrix} \beta u_2 \\ u_1u_2 \\ u_2u_2 + p \\ u_3u_2 \end{bmatrix}, \tilde{g} = \begin{bmatrix} \beta u_3 \\ u_1u_3 \\ u_2u_3 \\ u_3u_3 + p \end{bmatrix}$$

$$e^v = \begin{bmatrix} 0 \\ \tau_{xx} \\ \tau_{xy} \\ \tau_{xz} \end{bmatrix}, f^v = \begin{bmatrix} 0 \\ \tau_{xy} \\ \tau_{yy} \\ \tau_{yz} \end{bmatrix}, g^v = \begin{bmatrix} 0 \\ \tau_{xz} \\ \tau_{yz} \\ \tau_{zz} \end{bmatrix}, \tau_{ij} = \left(\frac{1}{Re} + \nu_t\right)\left(\frac{\partial u_i}{\partial x_j} + \frac{\partial u_j}{\partial x_i}\right)$$

V_i is a cell volume, S_x, S_y, S_z are area vector of each direction. E and E^v are inviscid and viscous flux, respectively. $Re\left(\equiv UL/\nu\right)$ is the Reynolds number where ν is the kinematic viscosity, U and L are the reference velocity and length, respectively. ν_t is the non-dimensional kinematic eddy viscosity which is determined by the Spalart-Allmaras one equation model[6].

The inviscid fluxes are evaluated by an upwind scheme based on the flux-difference splitting of Roe [7] with the second order accuracy by MUSCL. The viscous fluxes are discretized by second order centered differencing [8].

Euler backward implicit time marching scheme is employed for the time discretization.

III. Boundary Conditions

In order to calculate two-dimensional flows over a hill and a backward facing step, the following boundary conditions are implemented to SURF.

At the inlet boundary, u_1 , u_2 and ν_t are set to the prescribed values. The Neumann boundary condition is employed for p .

At the outlet boundary, u_1, u_2 and ν_t are the Neumann boundary condition, while p is set to zero.

At the wall boundary, no-slip condition is employed, that is, u_1, u_2 and ν_t are set to zero, while, p is the Neumann boundary condition.

IV. Uncertainty Estimation Procedure

The uncertainty estimation procedure which is proposed by Eca and Hoekstra [1],[2] is applied to the problems.

In order to neglect the iterative uncertainty, the calculations are continued until the residual of all variables reduce to machine zero.

V. Results

A. Flow over a hill: C-18

All the grids prepared for the Workshop are used for the uncertainty analysis. Therefore, 22 cases of calculations (11 grids with different density x 2 sets) are carried out.

1) Flow field

The contours of u_1, u_2, C_p and ν_t at the finest, medium and coarsest grids are depicted in Figure1. There are no significant differences between the results of the Set A and the Set B.

2) Uncertainty Analysis

The results of the uncertainty analysis are listed in Table 1. Note that the parameter p of Richardson extrapolation method, which denotes the order of accuracy, is also listed in this table. At three cases painted in red, the values of p are negative, thus the uncertainty values diverge by the present uncertainty analysis procedure. In order to investigate these divergences, the grid convergences for each variable are depicted in Figure 2 and 3.

In Figure 2, the convergence of the local flow quantities with the grid refinement at the three prescribed locations are shown. The convergence of the integral quantities with the grid refinement are shown in Figure 3.

In case of u_2 at x=5.357h and y=0.107h, the gradient becomes steep as the hi/h1 decreases, which yields the monotonic divergence. Grid resolutions seem to be insufficient.

B. Flow over a backward facing step: C-30

The grids of set B and C are used for the uncertainty analysis. 14 cases of calculations (7 grids with different density x 2 set) are carried out.

1) Flow field

The contours of u_1, u_2, Cp and ν_t at the finest, medium and coarsest grids are depicted in Figure 4. There are obvious differences between the results of Set B and C. Specifically, the distributions of u_2 , C_p and ν_t are different.

Behind the backward facing step, the u_2 of the Set B is higher and the C_p of the Set B is lower. On the other hand, the maximum value of the ν_t of the Set B is larger than that of the Set C. It can be considered that these differences are due to the different shapes of the steps. The shape of the step corner of the Set C is not the right angle, thus the characteristics of the backward facing step flow are weaken in these cases.

2) Uncertainty Analysis

The results of the uncertainty analysis are listed in Table2. At seven cases painted in red, the values of p are negative.

The convergence of the local flow quantities with the grid refinement at the three prescribed locations are depicted in Figure 5. The convergence of the integral quantities with the grid refinement are depicted in Figure 6.

In the case of the C_p at the location of x=0 and h=1.1h, the p value of the Set C is negative and that of B is positive. In this case, the values of C_p of the Set C are nearly constant compared to the Set B, and these values appear to be converged. However, the obtained value of the p by using the least square method becomes negative and the convergence state is determined to be the monotonic divergence.

In the case of the $C_{p\ bottom}$ of the Set C, the similar problem also happens.

VI. Discussion

In our calculations of the case C-30, seven cases of the uncertainty values are computed to be divergent. In the first step, we investigate the convergence of the flow field visually, in order to make sure our Navier-Stokes equation solver computes flow fields properly. Streamlines and contours of pressure with the C-30 grids are shown in Figure 7. Two streamlines are plotted in each figure. One

streamline passes through the point x=0 and y=1.1h, and the other one passes through the point x=1.0h and y=0.1h. The latter streamline is circulating. The interval of the circulated streamlines becomes small as the density of the grids increases. This shows that the flow field is converging, as the grids become fine.

In the next step, we assume that the negative values of the *p* of the local quantities are due to the fact that the results are out of the asymptotic region. In order to verify the hypothesis, we defined the new analysis point 2' that locates nearer to the wall than the point 2 and carried out the uncertainty analysis for this point. The coordinates of the point 2' is x=h and y=0.005h and depicted as shown in Figure 8. The results of uncertainty analysis of the point 2' are shown in Table 3 and Figure 9. All the values of *p* of the point 2' become positive. We can consider that the density of the grids around point 2' is in the asymptotic region, while that of point 2 is not sufficient. Although the case of the point 2' is only one example, it can be concluded that the uncertainty analysis for the local quantities should be carried out at the locations with higher grid density than the present locations.

VII. CONCLUSIONS

Two-dimensional flows over a hill and a backward facing step are calculated with the Navier-Stokes solver SURF. All the grids cases except the Set A of the C-18 are used for the calculations. For the turbulence model, one-equation model of Spalart and Allmaras is employed. In order to neglect the iterative uncertainty, the calculations are continued until the residual of all variables reduce to machine zero.

In the case C-18, the calculated results of Set A and B are similar, on the other hand, in the case C-30 the flow fields of Set B and C are obviously different because the shapes of the corner of the step are different.

For the uncertainty analysis, the procedure proposed by Eca and Hoekstra is employed. Generally, the values of the uncertainty can be obtained, however, the uncertainty values of ten cases are divergent. In the cases of uncertainty analysis of the local quantities, the main reason of the divergence is considered that the density of the grid is not high enough for the solutions to be in the asymptotic region.

REFERENCES

[1] L.Eca, and M.Hoekstra, "Uncertainty Estimation: A Ground Challenge for Numerical Ship Hydrodynamics," Proc. 6th Numerical Towing Tank Symposium, Rome, 2003

[2] L.Eca, and M.Hoekstra, "An Evaluation of Verification Procedures for CFD Applications", Proc. 24th Symp. on Naval Hydrodynamics, Fukuoka, 2002

[3] P.J.Roache, "Verification and Validation in Computational Science and Engineering", Hermosa Publishers, 1998

[4] T.Hino, "A 3D Unstructured Grid Method for Incompressible Viscous Flows," J. Soc. of Naval Archit. Japan, Vol 182, 1997,pp.9-15

[5] A.J.Chorin, "A Numerical Method for Solving Incompressible Viscous Flow Problems", J. Comput. Pys., Vol.2, 1967, pp.12-26

[6] P.R.Spalart, et al., "A One-Equation Turbulence Model for Aerodynamic Flows", La Recherche Aèrospatiale, No.1, 1994, pp.5-21

[7] P.L.Roe, "Characteristic-based scheme for the euler equations," Ann. Rev. Fluid Mech., Vol.18, 1986, pp.337-365

[8] T. Hino, "Navier-Stokes Computations of Ship Flows on Unstructured Grids," Proc. of the 22nd Symp. on Naval Hydro., 1998, pp.463-475

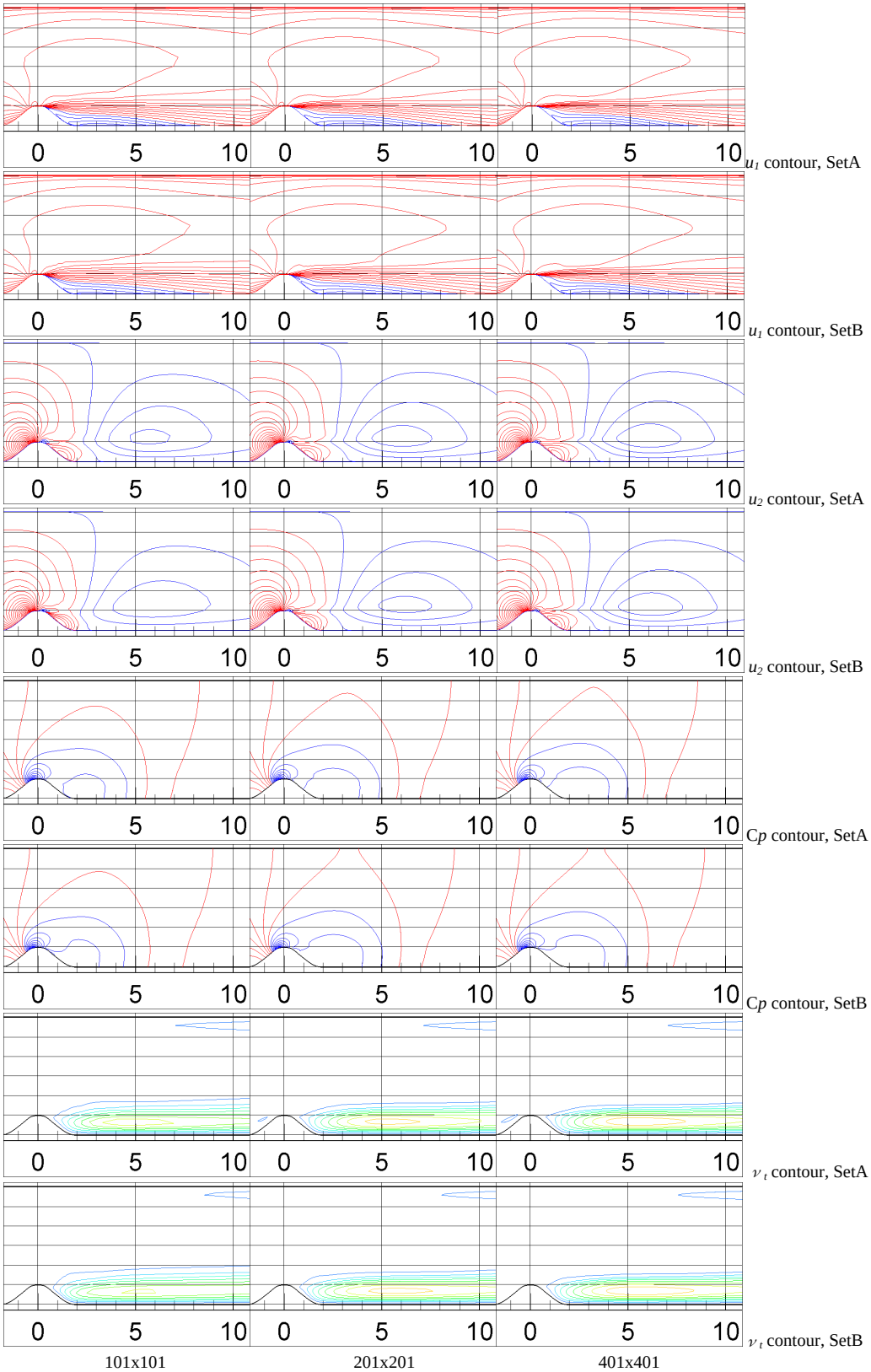

Figure 1: Calculated results of the flow field (C-18)

[u_1: The interval of the contours=0.1, red lines: positive, blue lines: negative], [u_2: The interval of the contours =0.025, red lines: positive, blue lines: negative], [C_p : The interval of the contours =0.1], [ν_t: The interval of the contours=0.002]

Table 1: Results of uncertainty analysis, case C-18

	Variables	x=0,y=1.25h		x=2.5h,y=0.25h		x=5.357h,y=0.107h	
		Set A	Set B	Set A	Set B	Set A	Set B
Local flow quantities	u_1	1.169E+00	1.166E+00	-2.085E-01	-2.104E-01	-1.953E-01	-2.004E-01
	Uncertainty of u_1	3.171E-03	5.060E-04	1.140E-02	7.647E-04	4.798E-03	1.055E-02
	p of u_1	1.28	3.03	0.55	4.18	2.01	1.70
	u_2	1.142E-01	1.161E-01	1.475E-02	1.317E-02	-1.077E-02	-1.008E-02
	Uncertainty of u2	2.331E-03	4.025E-04	2.306E-03	1.456E-02	Divergence	Divergence
	p of u_2	1.43	2.73	0.87	0.54	-1.59	-1.03
	C_p	-6.506E-01	-6.432E-01	-4.688E-01	-4.720E-01	-2.446E-01	-2.538E-01
	Uncertainty of Cp	6.572E-03	1.236E-03	9.154E-03	2.492E-03	3.579E-03	4.819E-03
	p of C_p	1.56	3.05	1.20	2.13	2.41	2.96
	ν_t	1.872E-03	1.860E-03	6.251E-03	6.313E-03	2.803E-03	2.772E-03
	Uncertainty of ν_t	9.144E-05	8.244E-05	4.183E-05	4.482E-04	3.659E-04	1.007E-03
	p of ν_t	0.89	0.99	3.64	0.61	0.38	0.47

	Variables	Set A	Set B
Integral quantities	Cf b[*1]	2.316E-02	2.279E-02
	Uncertainty of Cf b	2.575E-04	7.030E-04
	p of Cf b	1.33	0.68
	Cf t[*2]	5.563E-02	5.575E-02
	Uncertainty of Cf t	9.513E-05	1.689E-04
	p of Cf t	2.98	1.24
	Cp b[*3]	1.908E-01	1.941E-01
	Uncertainty of Cp b	4.590E-03	7.988E-04
	p of Cp b	1.10	3.46

Cf b[*1]: Frictional resistance at bottom wall

Cf t[*2]: Frictional resistance at top wall

Cp b[*1]: Pressure resistance at bottom wall

	Variables	Set A	Set B
Integral quantities	X sep.[*4]	2.114E-01	2.051E-01
	Uncertainty of X	9.596E-03	1.149E-03
	p of X sep.	1.25	2.67
	X reat.[*5]	8.407E+00	8.533E+00
	Uncertainty of X	2.909E-01	Divergence
	p of X reat.	4.56	-2.61

X sep.[*4]: Separation point

X reat.[*5]: Re-attachment point

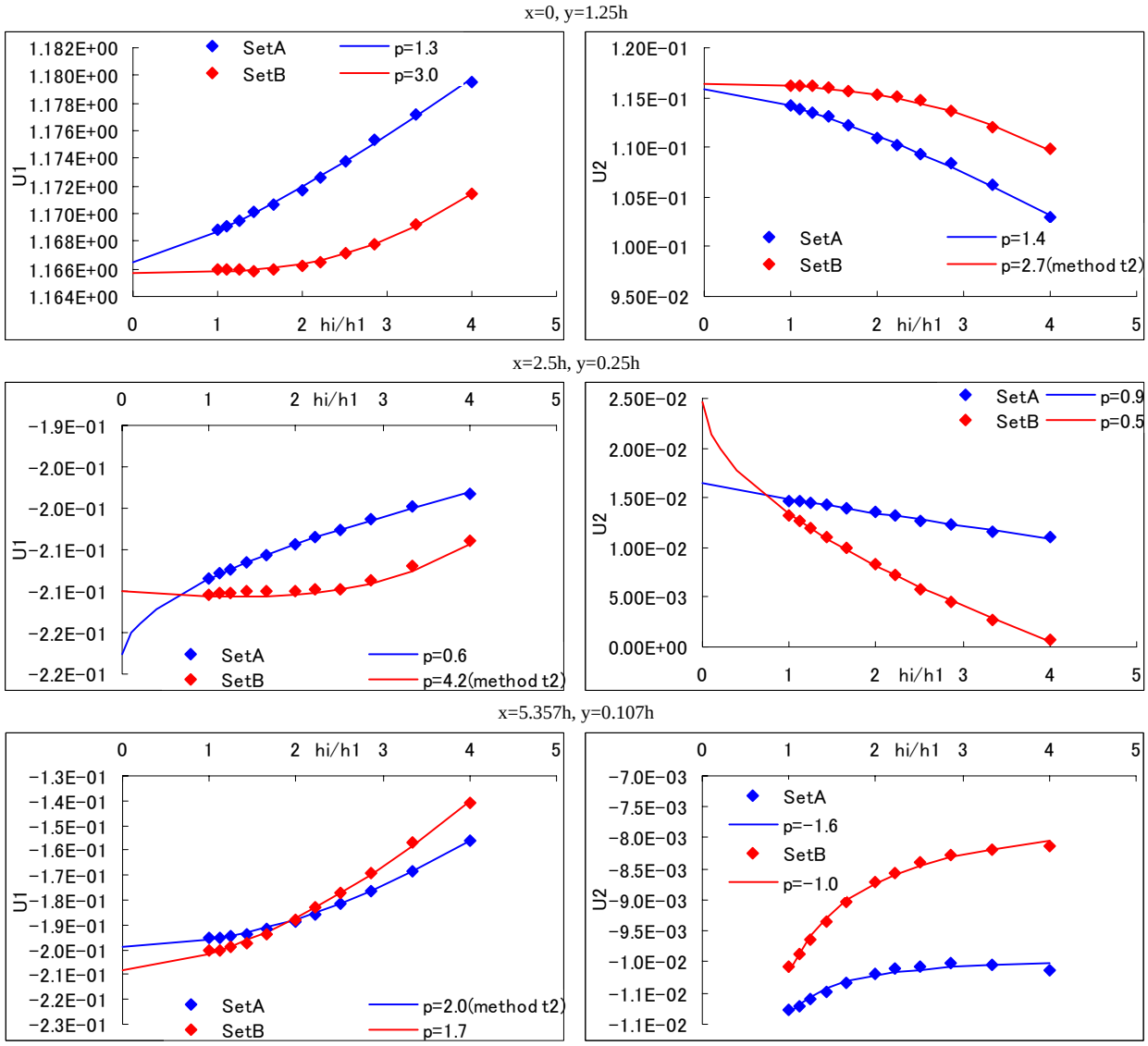

Figure 2: Convergence of the local flow quantities with the grid refinement at the three prescribed points. (C-18)

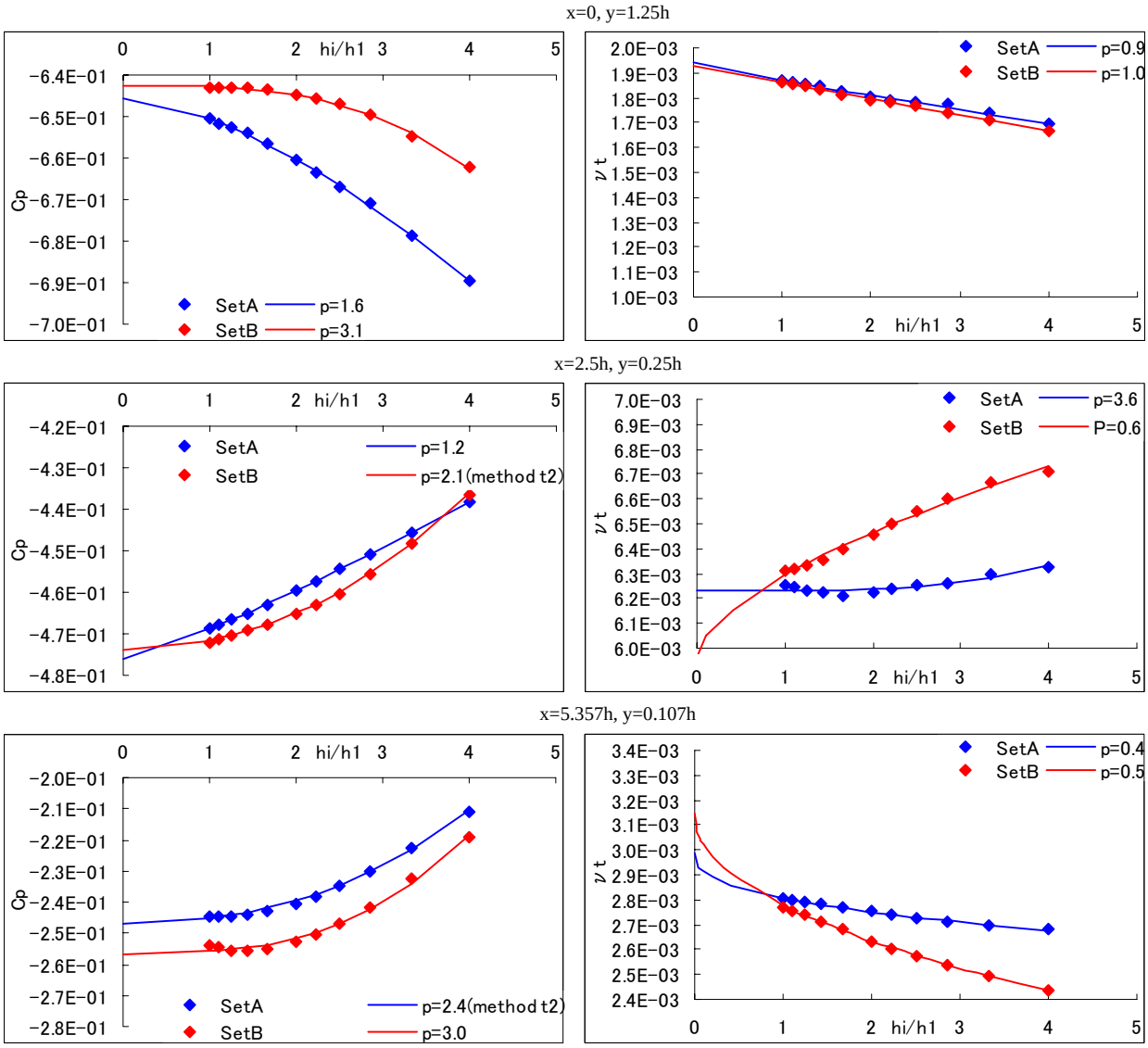

Figure 2(Continue): Convergence of the local flow quantities with the grid refinement at the three prescribed points. (C-18)

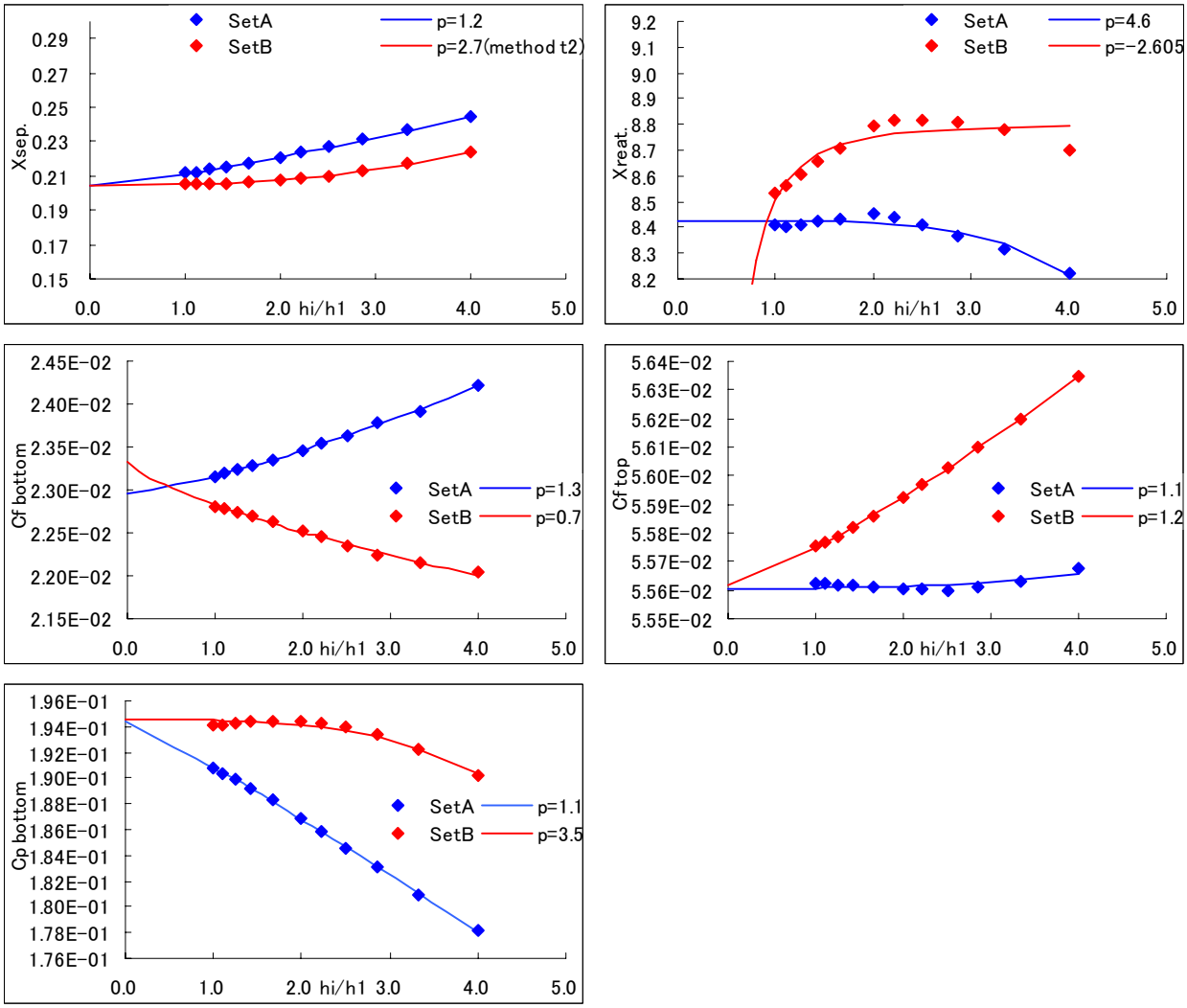

Figure 3: Convergence of the integral quantities with the grid refinement. (C-18)

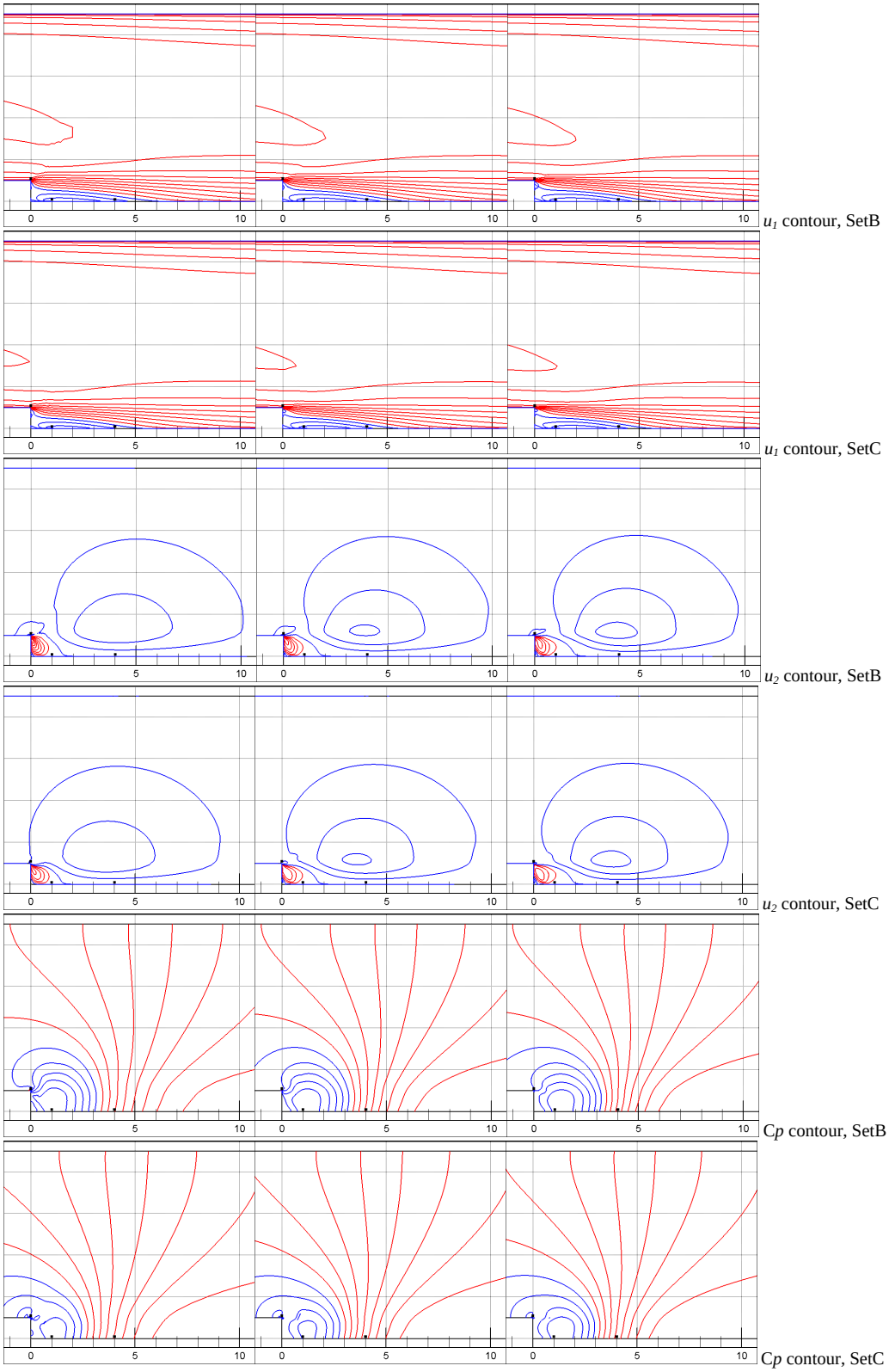

Figure 4: Calculated results of the flow field (C-30)

[u_1: The interval of the contours=0.1, red lines: positive, blue lines: negative], [u_2: The interval of the contours =0.025, red lines: positive, blue lines: negative], [C_p : The interval of the contours =0.1]

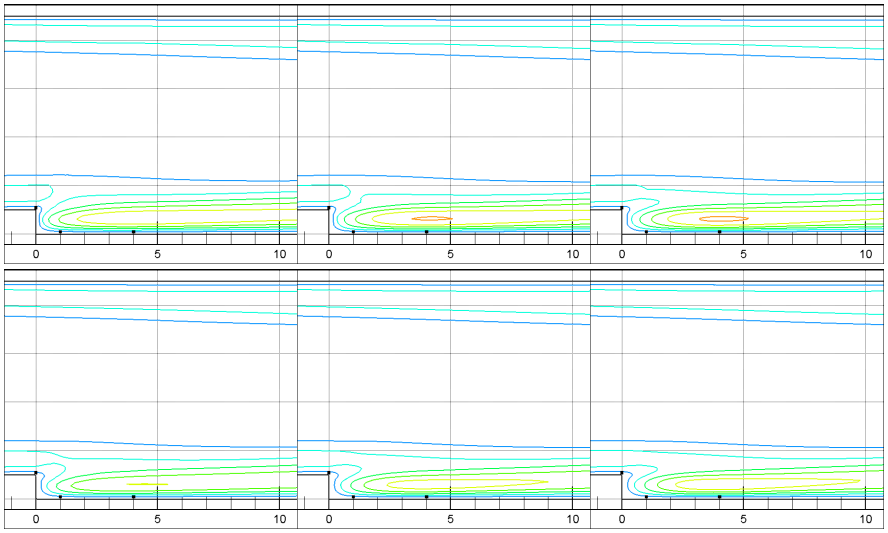

Figure 4 (Continue): Calculated results of the flow field (C-30)

[ν_t: The interval of the contours=0.002]

Table 2: Results of uncertainty analysis, case C-30

	Variables	x=0,y=1.1h		x=h,y=0.1h		x=4h,y=0.1h	
		Set B	Set C	Set B	Set C	Set B	Set C
Local flow quantities	u_1	6.751E-01	6.857E-01	-2.216E-01	-2.079E-01	-1.097E-01	-8.619E-02
	Uncertainty of u_1	3.172E-02	1.458E-01	Divergence	1.519E-02	6.483E-03	3.341E-02
	p of u_1	0.70	5.83E-05	-0.20	0.17	1.33	1.07
	u_2	6.515E-03	-1.817E-02	1.175E-02	1.323E-02	-9.740E-03	-1.026E-02
	Uncertainty of u2	4.382E-02	Divergence	Divergence	1.325E-02	5.763E-03	2.927E-04
	p of u_2	0.29	-0.44	-0.17	0.43	0.16	2.86
	C_p	-1.761E-01	-1.997E-01	-2.463E-01	-2.265E-01	-9.354E-02	-7.420E-02
	Uncertainty of Cp	3.921E-02	Divergence	Divergence	8.401E-03	2.530E-02	9.613E-03
	p of C_p	0.92	-2.00	-0.51	1.28	0.21	1.28
	ν_t	1.425E-03	1.359E-03	1.373E-03	1.317E-03	2.079E-03	2.062E-03
	Uncertainty of ν_t	5.182E-05	8.295E-05	3.806E-04	1.015E-04	3.477E-04	Divergence
	p of ν_t	0.71	3.22	0.11	1.07	0.55	-0.15

	Variables	Set B	Set C
Integral quantities	Cf b[*1]	2.583E-02	2.649E-02
	Uncertainty of Cf b	4.511E-04	2.862E-05
	p of Cf b	1.47	2.24
	Cf t[*2]	4.752E-02	4.754E-02
	Uncertainty of Cf t	9.698E-05	1.281E-04
	p of Cf t	1.99	1.81
	Cp b[*3]	1.073E-01	1.006E-01
	Uncertainty of Cp b	7.215E-03	Divergence
	p of Cp b	0.92	-2.08E-04
	X reat.[*4]	6.155E+00	5.885E+00
	Uncertainty of X	1.080E+00	4.555E-02
	p of X reat.	0.31	2.60

Cf b[*1]: Frictional resistance at bottom wall

Cf t[*2]: Frictional resistance at top wall

Cp b[*3]: Pressure resistance at bottom wall

X reat.[*4]: Re-attachment point

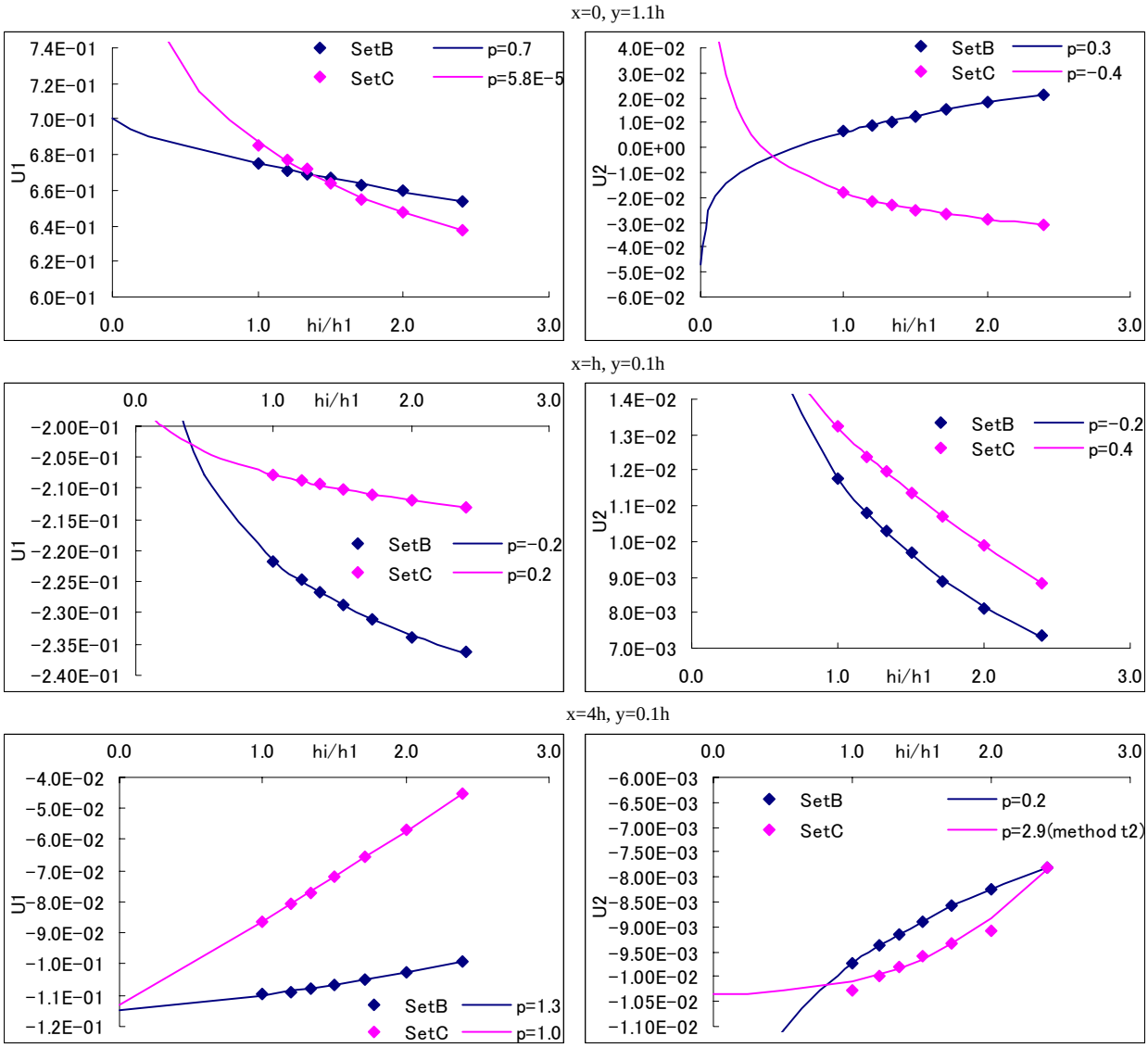

Figure 5: Convergence of the local flow quantities with the grid refinement at the three prescribed points. (C-30)

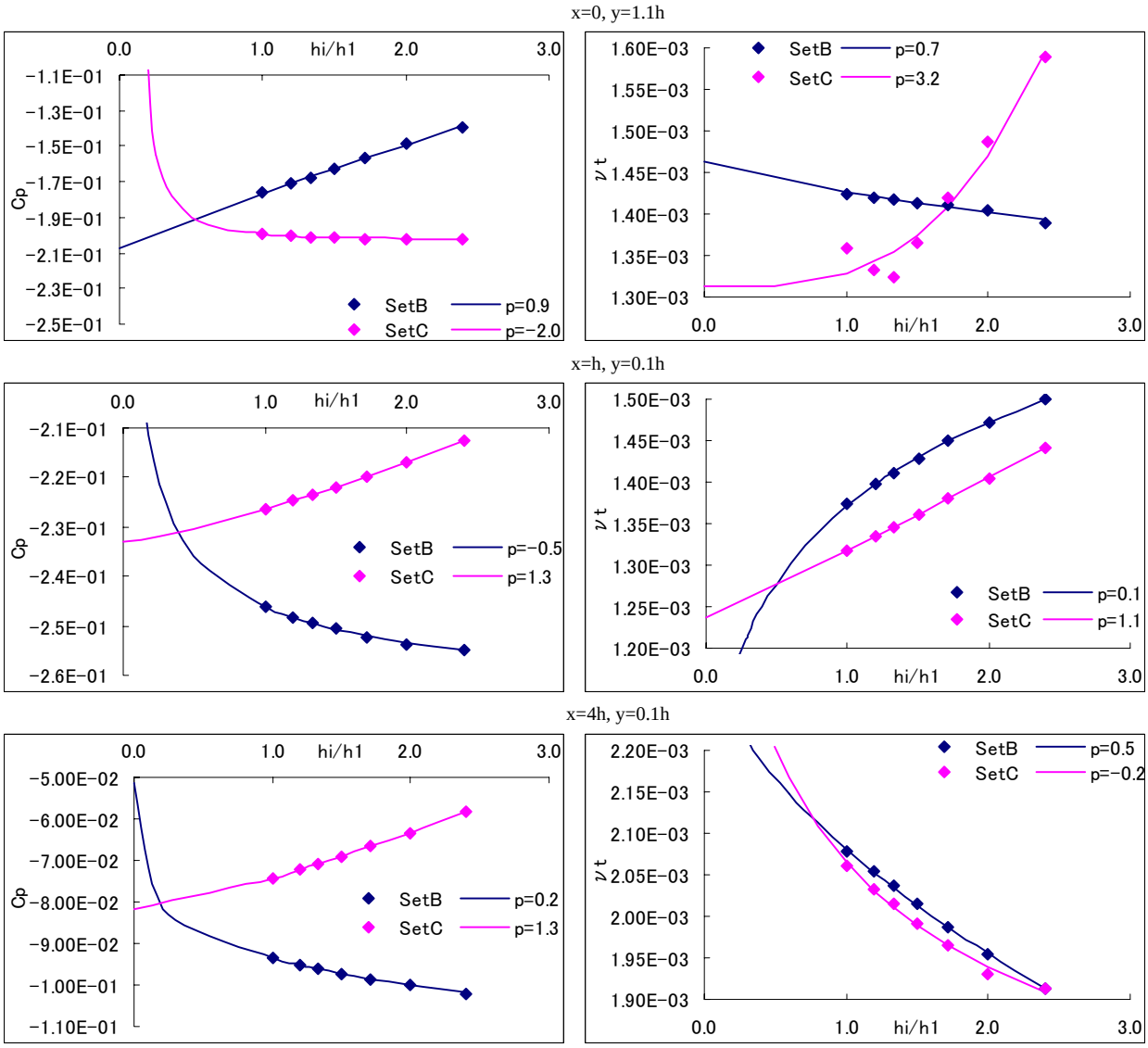

Figure 5 (Continue): Convergence of the local flow quantities with the grid refinement at the three prescribed points. (C-30),

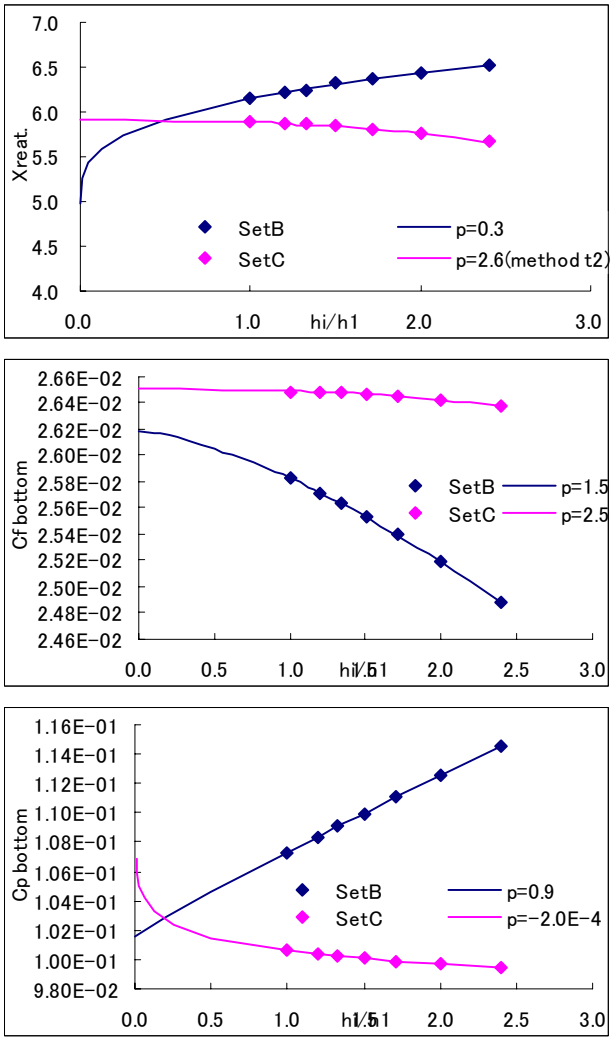

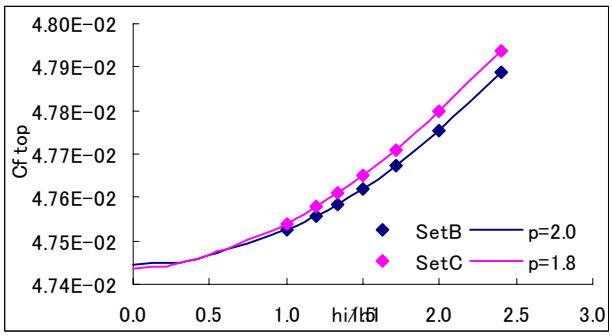

Figure 6: Convergence of the integral quantities with the grid refinement. (C-30)

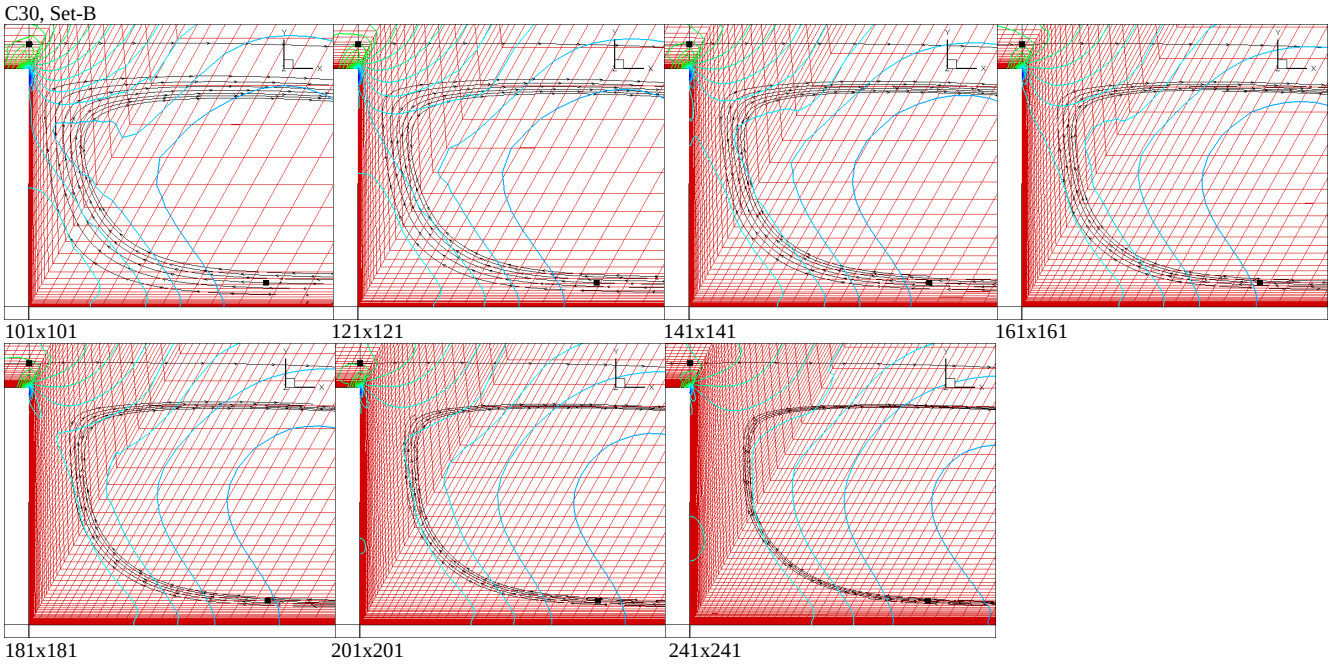

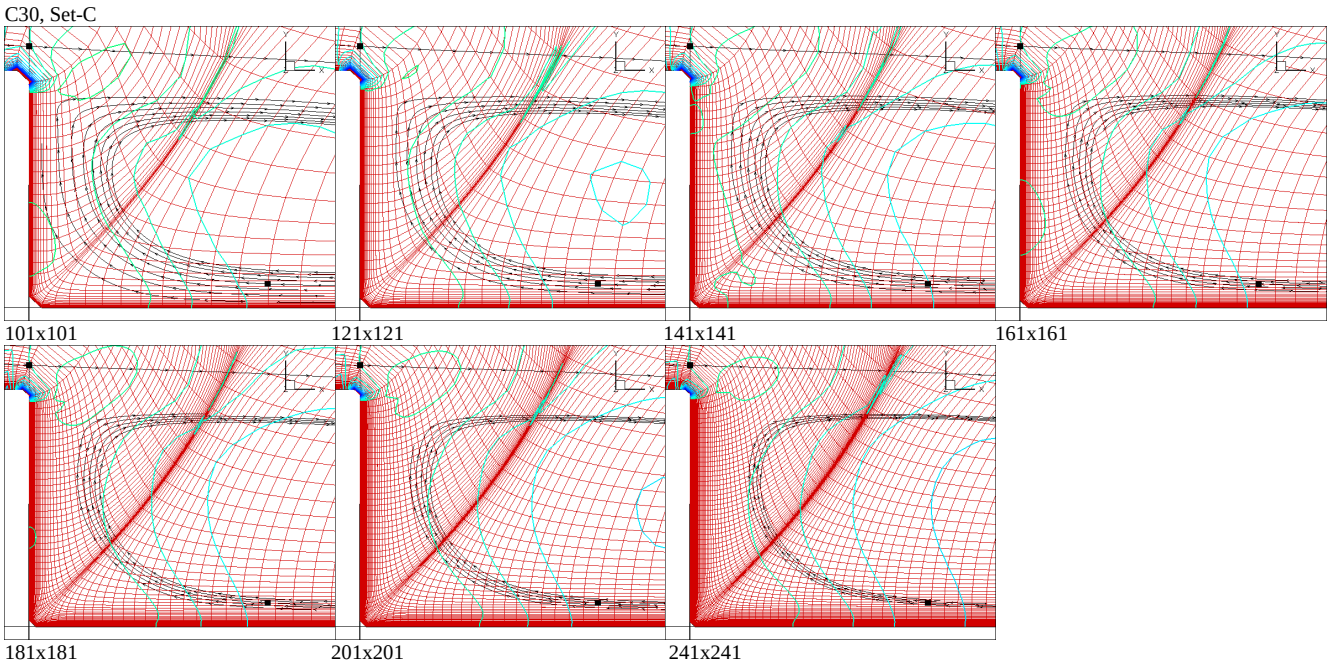

Figure 7: Computational grids and the calculated results of the pressure contour and two streamlines around the backward facing step. The interval of the pressure contour is 0.1. One streamline passes the point (0.0, 1.1h) and the other passes the point (1.0h, 0.1h).

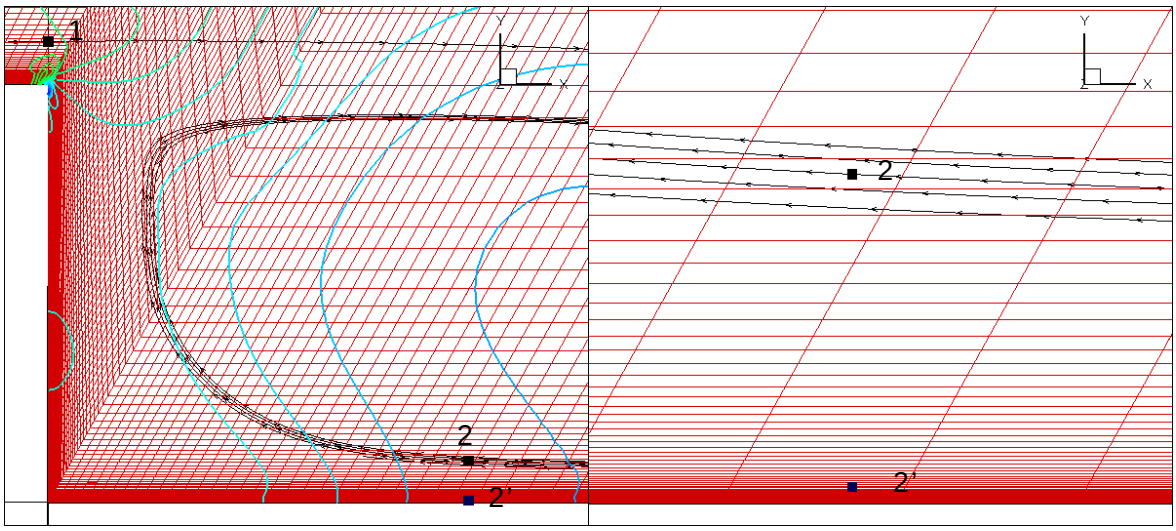

Figure 8: Definition of the new analysis point 2'.

point2: (x,y)=(1.0h,0.1h), point2':(x,y)=(1.0h,0.005h)

Table 3: Comparison of the *p* values between the point2 and 2'.

Variables		point2 (x=h,y=0.1h)		point2' (x=h,y=0.005h)	
		Set B	Set C	Set B	Set C
Local quantities	u_1	-0.20	0.17	4.40	0.43
	u_2	-0.17	0.43	3.16	2.98
	C_p	-0.51	1.28	4.32	1.31
	ν_t	0.11	1.07	1.03	1.02

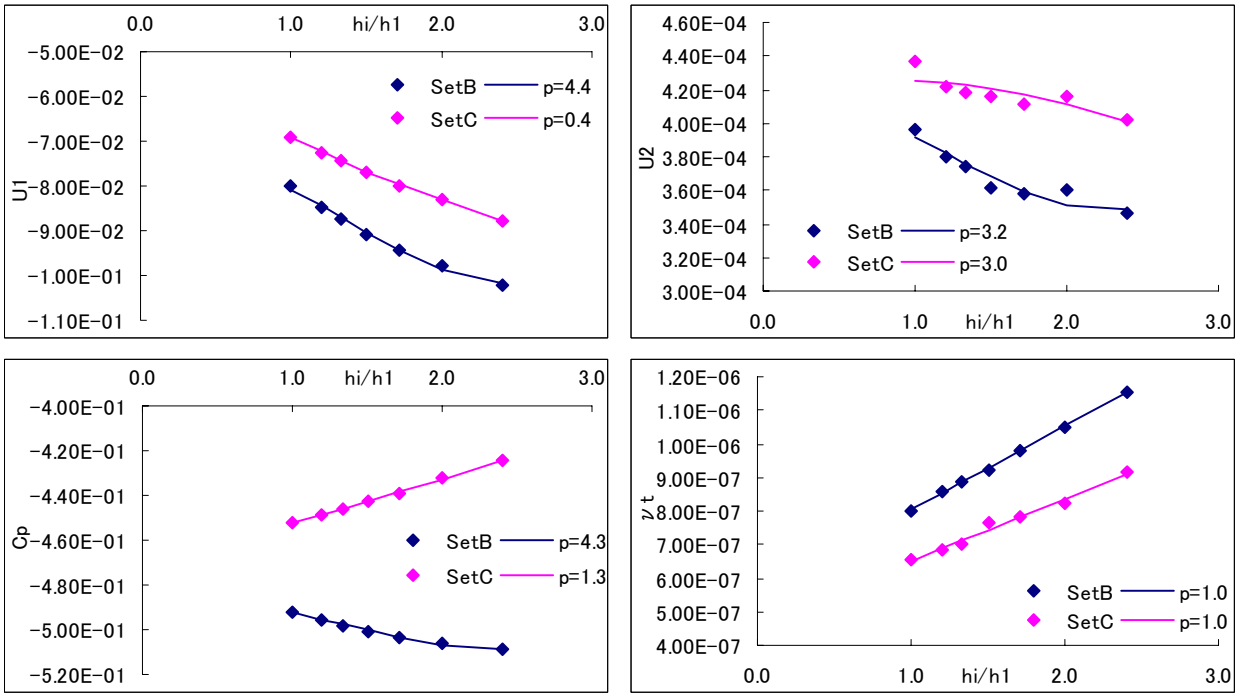

Figure 9: Convergence of the local flow quantities with the grid refinement at the points2'. (C-30)